Modelling and design of tracked mobile climbing robots on non-planar surfaces

Stephen L. Canfield, Padmanabhan Kumar and Joshua E. Qualls*

Department of Mechanical Engineering,
Brown Hall 224, 115 W. 10th Street,
Cookeville, TN 38505, USA
Email: scanfield@tntech.edu
Email: padmanabhankumar@gmail.com
Email: jequalls21@students.tntech.edu
*Corresponding author

Abstract: This paper presents an analysis of a tracked-based skid steer mobile robot following a defined path on a class of non-planar surfaces. The analysis will define a method to approximate the position and orientation of each track on a climbing surface in a manner that ensures opposing, symmetric components of the robot are geometrically even in their positioning relative to the base surface. The analysis will assume the robot chassis travels along the path with an orientation defined by the vectors tangent to the path and normal to the climbing surface, and that the centerline distance and longitudinal displacements between the tracks units are fixed. It will be shown that for general paths, three rotational degrees of freedom are required between the tracks to maintain line contact with the surface along the length of the track. This implies that the tracks do not remain parallel while following paths on non-planar surfaces. It will further be shown that relative lateral slipping between the left and right tracks result when traversing non-planar surfaces. Two subsets of paths are shown to require one rotational degree of freedom only and avoid lateral slipping. The model will then be used to define the required relative motion between the tracks which can be used to design a kinematic arrangement for connecting track modules to a central chassis in a manner to minimise slip and maximise surface contact when climbing on non-planar surfaces.

Keywords: climbing; mobile robot; non-planar; skid steer; tracks.

Reference to this paper should be made as follows: Canfield, S.L., Kumar, P. and Qualls, J.E. (2017) 'Modelling and design of tracked mobile climbing robots on non-planar surfaces', *Int. J. Mechanisms and Robotic Systems*, Vol. 4, No. 1, pp.24–42.

Biographical notes: Stephen Canfield is a Professor in the Department of Mechanical Engineering and T.S. McCord Faculty Fellow in Innovation and Techno-Entrepreneurship at Tennessee Technological University. He received his Ph.D. in Mechanical Engineering at Virginia Tech in the field of parallel architecture robotics. His current research is in robot modelling, control and development with a focus on climbing mobile robots for autonomous welding and NDE inspection in hazardous, unstructured environments.

Padmanabhan Kumar is a Licensed Engineer working on self-driving cars and has been instrumental in getting robotic systems implemented in automobiles. He was a graduate student from 2010 to 2012 on mobile robotic systems and

received his Master's in Mechanical Engineering from Tennessee Technological University on robotic systems in the field of autonomous vehicles.

Joshua Qualls received his Master's of Science in Mechanical Engineering from Tennessee Technological University in 2016 and works in the vehicle engineering and manufacturing industry.

1 Introduction

Efforts to design mobile robots for manufacturing and service industries are increasing because of the safety, accuracy and other operational benefits provided by these systems. Mobile robots that are capable of climbing while performing manufacturing/service tasks form a subcategory of this group. Towards this end, a variety of wheeled, tracked and legged climbing robots have been demonstrated in the literature (Yan and Shuliang, 1999; Kim et al., 2008; Fischer et al., 2008; Xu and Ma, 2002; Shen et al., 2005; Kumar et al., 2011; O'Toole and Canfield, 2010). Many of these robots have been demonstrated for their use in welding, cutting, inspection and other industrial operations. These operations generally require the mobile robot to traverse a surface along a path while performing a task. In an idealised sense, the surface is treated as planar or having small surface variations (such as a weld seam or a rivet) that could be generally ignored in a macro-model of the system. However, in practice, such surfaces are very rare. When considering the types of structures that might be treated with these robots, such as ship-hulls, boilers, storage tanks and windmills, it becomes apparent that the planar surface model is not representative. The robot must comply with the geometry of the climbing surface in order to remain stable and perform the desired operation. Thus, the climbing surface affects the design of the robot. This paper presents a model to design a mobile climbing robot system for operation on non-planar surfaces. This work applies to a group of climbing robots - skid steer mobile robots (SSMR) with a focus on track-type SSMRs.

The subject of design of mobile robots for traversing non-planar or uneven terrain has been widely considered in the literature. By their nature, legged mobile robots naturally encompass the ability to move over a surface through leg placement (Letourneau and Arsenault, 2003; Raibert and Blankespoor, 2008; Hoggins, 1988). When considering wheeled systems, a number of studies have investigated wheeled mobile robots (WMR) when traversing uneven terrain (Davis et al., 1997; Sreenivasan and Nanua, 1996; Chakraborty and Ghosal, 2004). One of the primary considerations in this work is analysis of lateral slip (Davis et al., 1997) and development of mechanisms to avoid this slip (Hoggins, 1988) and to consider realistic wheel models on uneven terrain (Sreenivasan and Nanua, 1996). Conversely, when considering SSMRs, wheel or track type, slipping becomes a necessary condition of operation on any surface, planar or non-planar (Chakraborty and Ghosal, 2004). Models to estimate this slip at the kinematic level have been demonstrated (O'Toole and Canfield, 2010; Mandow et al., 2007), but this only considers slipping due to operation on planar surfaces. There is little evidence of models that consider the additional slip behaviour of SSMRs when operating on non-planar, uneven surfaces.

This paper presents an analysis of a tracked-based SSMR following a defined path on a class of non-planar surfaces. The analysis will present a method to approximate the position and orientation of each track on a climbing surface in a manner that provides

geometric stability, where geometric stability is defined as a condition in which opposing, symmetric components of the robot are geometrically even in their positioning relative to the base surface. The analysis will assume the robot chassis is centred and directed along the path and that the centerline distance and longitudinal displacements between the tracks units are fixed. It will be shown that for general paths, three rotational degrees of freedom are required, implying that the tracks would not remain parallel while following even simple paths on non-planar surfaces. It will further be shown that lateral slipping between the left and right tracks results when traversing non-planar surfaces as has been established for wheeled-type robots (Sreenivasan and Nanua, 1996; Chakraborty and Ghosal, 2004). Two subsets of paths are shown to require one rotational degrees of freedom only (vertical and horizontal) and avoid lateral slipping. The model will then be used to define the range of relative motions between the tracks during a typical operation. This model can be used to aid the design of the kinematic arrangement for connecting track modules to a central chassis in a manner to minimise slip and maximise surface contact when climbing on non-planar surfaces.

2 Approach

A representative configuration of a track-based skid-steer mobile robot is the mobile robot welding system (MRWS) presented in O'Toole and Canfield (2010) and shown in Figure 1 performing a welding operation. The MRWS consists of a chassis and two magnetic track units for adhering to steel surfaces, shown schematically in Figure 2. The track units contain a drive system and continuous chain with permanent magnetic feet attached. The track units also contain a suspension that allows the track to conform to the variations on the base surface as shown in Figure 3. A frame $\{x_{ro}, y_{ro}, z_{ro}\}^{T}$ is attached to the centre of the robot chassis at point $\mathbf{C_r}$ with x_{ro}, y_{ro} directed along the robot longitudinal and lateral directions, respectively, as shown in Figure 2 and z_{ro} completing the frame (Figure 3).

Figure 1 Mobile robotic welding system performing a welding operation (see online version for colours)

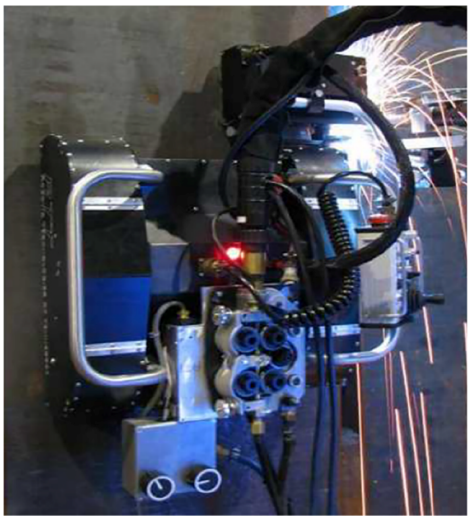

Figure 2 Schematic of MRWS chassis and tracks

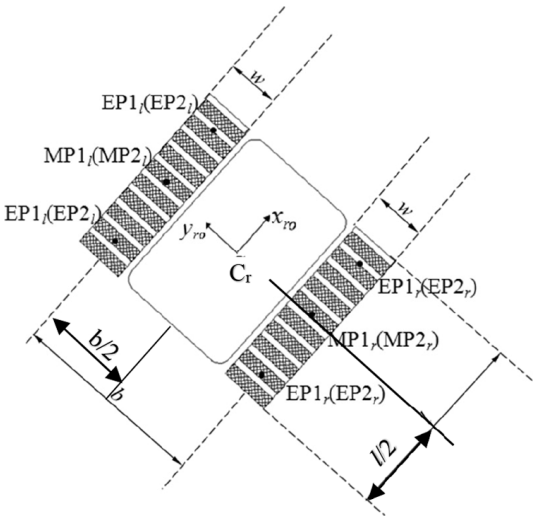

Figure 3 Side view of MRWS tracks accommodating surface irregularities

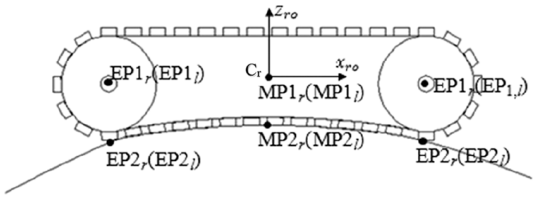

For the purposes of this paper, the left and right track units of the MRWS are attached to a rigid chassis in a manner such that they can achieve independent orientation in three directions (pitch, roll and yaw) with respect to each other. It is assumed that the distance between the centre of the left and right track units are constant. Additional assumptions are that the radius of the track sprockets are small relative to the radius of curvature of the traversing surface (base surface) and the width of track, w, is considered to be negligible relative to the other key robot dimensions, b and l.

Next consider the MRWS on a non-planar surface as shown in Figure 4. This surface is called the base surface and for the purpose of this analysis, it will be considered as an extrusion of a closed curve along the global Z-axis to yield a right cylinder. The inertial reference frame is defined by $[X, Y, Z]^{\mathrm{T}}$ with Z lying along the axis of extrusion of the surface and the X- and Y-axes lying in the base of the cylinder. For the remainder of this description, the base surface will be considered to be a right circular cylinder as

$$x^2+y^2 = R^2 \,, \forall z \tag{1}$$

Figure 4 Mobile robot welding system on base surface (see online version for colours)

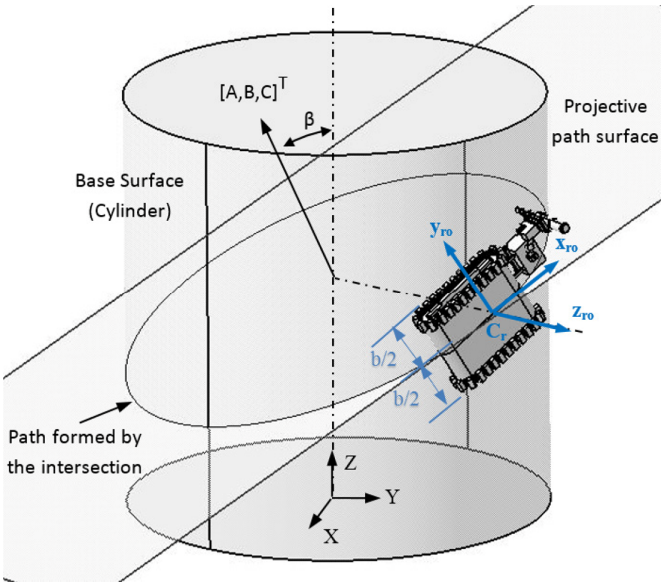

with x, y and z defined in the inertial frame. The robot will traverse the base surface to complete an assigned task. The robot task is defined by a path specified on the base surface. This path will be specified as the intersection of a projective path plane with the base surface. The projective path plane is described as $Ax + By + Cz + D = 0$. This plane will be considered as the projective path surface (Figure 4) and the base surface cylinder will project far enough to ensure that the intersection is a closed curve. Thus, a single parameter, β (the angle between the projective path surface and the base plane of the base surface) is sufficient to define the projective path surface. While not unique, this means of specifying the path is intuitive in practice, for example on a task of traversing a weld seam defined by the intersection of a plane with the base surface. Thus, the locus of points that define the robot path are given as,

$$y = -\frac{B(D+Cz) \pm A\sqrt{A^2R^2 + B^2R^2 - C^2z^2 - 2CDz - D^2}}{A^2 + B^2}, \tag{2}$$

$$x = \pm\sqrt{R^2 - y^2}\ , \tag{3}$$

$$\forall z = \left[\left(\frac{D + R\left(A^2 + B^2\right)^{\frac{1}{2}}}{C}\right), -\left(\frac{D - R\left(A^2 + B\right)^{\frac{1}{2}}}{C}\right)\right] \tag{4}$$

Note that two points of intersection are obtained simultaneously for every value of that is in the interior of the set z. The robot path is formed by ordering the points first along the positive solutions for Eq. (4) from $z = \left(D + R\left(A^2 + B^2\right)^{\frac{1}{2}}\right) \Big/ C$ to

$z = -\left(D - R\left(A^2 + B^2 \right)^{\frac{1}{2}} \right) \Big/ C$, and then along the negative solutions for Eq. (4) from $z = -\left(D - R\left(A^2 + B^2 \right)^{\frac{1}{2}} \right) / C$ to $z = \left(D + R\left(A^2 + B^2 \right)^{\frac{1}{2}} \right) \Big/ C$. A representative path thus obtained is shown in Figure 4 as an ellipse when viewed in the projective path plane. In this work, it is assumed that the origin of the robot chassis frame follows this path. The robot chassis frame $\{x_{ro}, y_{ro}, z_{ro}\}^{\mathrm{T}}$ is defined as the Frenet-Serret frame with x_{ro}, y_{ro}, z_{ro} the tangent, normal and binormal unit vectors, respectively. The motion of this frame is further defined by the Frenet formula as $dx_{ro}/ds = \kappa z_{ro}$, $dz_{ro}/ds = -\kappa z_{ro} + \tau y_{ro}$ and $dy_{ro}/ds = -\tau x_{ro}$ where s is a coordinate measuring travel along the path, κ the path curvature and τ the path torsion. For the path as defined, κ and τ are given as $= \frac{1}{aa^2 bb^2}\left(\frac{x^2}{aa^4} + \frac{y^2}{bb^4} \right)^{\frac{-3}{2}}$, $\tau = 0$ with aa and bb representing the major and minor axes, respectively, of the ellipse.

2.1 Idealised robot model

An idealised model of a tracked SSMR travelling along the defined path is first considered. This model assumes the robot dimensions, b, l are much smaller than the base surface radius, R, such that the surface appears to be locally planar to the robot. The result is that the left and right track frames share the same orientation as the chassis frame and are offset by $\pm b/2$ along the y_{ro}-axis. Thus, the left and right track frames can be assumed to follow paths defined by intersecting path planes parallel but offset from the projective path plane for the robot chassis by $\pm b/2$ along the y_{ro}-axis (Figure 4) and defined in the same manner as the chassis frame. At any point in time, the origins of the left and right track frames lie on the intersection of the y_{ro}–z_{ro} plane with the corresponding path for the left/right tracks. The base surface is now unwrapped to result in a rectangular, planar sheet. The cylindrical base surface unfolds along a line that will be called the x-axis while the paths unfold along sinusoidal curves defined as (Apostol and Mnatsakanian, 2007).

$$u_i(x) = R\tan(\beta)\sin\left(\frac{x}{R}\right) + C_i \tag{5}$$

where $i=rc$, l, r for the robot chassis, left and right track frames, respectively, and C_i the offset in the z-direction. These curves are shown in Figure 6, where the vertical, y, axis is obtained using Eq. (5) and the horizontal, x, axis is the arc length, $R\theta$, of the cylindrical surface when unwrapped. Thus, while travelling along a path (plane intersecting a cylinder) on a cylindrical base surface, the robot must travel along a sinusoidal curve when viewed on the wrapped surface. The amplitude of the curve is proportional to $R\tan\beta$, goes to zero when β is zero and goes to infinity when β goes to $\pi/2$. Thus, the robot only follows a straight line when travelling vertically or horizontally along the cylinder base. For all other paths, the robot is in a continual state of turning. For SSMRs, this means that the robot will be operating at a high torque input rate for all but a small subset of tasks on a non-planar surface.

Figure 5 Parallel planes defining paths for simplified model (see online version for colours)

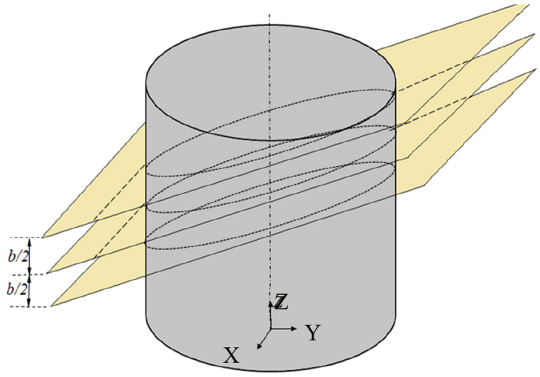

Figure 6 Path of idealised model on unwrapped surface

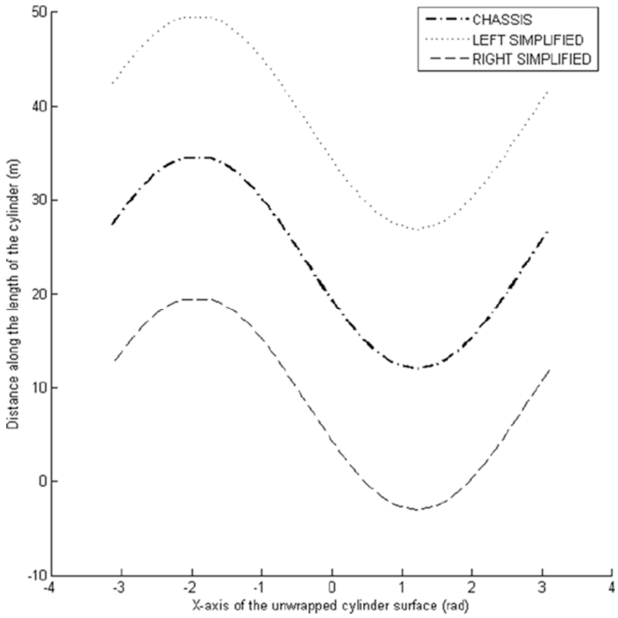

For the tracked SSMR, it is well known that slip is required for turning (Mandow et al., 2005). This arises from two effects which are considered here. The first is slip resulting from line contact between the track and the surface. Following the model provided in Mandow et al. (2005), an approximation of this slip and resulting friction and track torques can be evaluated as follows. Consider a schematic of the track system as shown in Figure 7 where $F_{r,x}$, $F_{l,x}$ and F_y are the friction forces at the left/right tracks in the local x-, y-directions and x_{ic}, y_{lic}, y_{ric} represent the instant centres of motion associated with the left and right track contact patches, respectively. The instant centres fall on a line orthogonal to the track according to Kennedy's theorem.

Figure 7 Static model to define friction forces

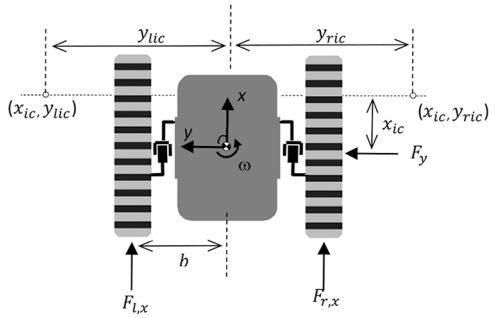

The friction forces arise at the intersection of the track and climbing surface interface. A coulomb friction model is assumed and furthermore a uniform normal force resulting from the magnetic attraction is defined between the track and climbing surface to yield friction forces as follows:

$$F_{l,x} = -\mu N \frac{-\left(b - y_{lic}\right)}{\sqrt{\left(b - y_{lic}\right)^2 + \left(x_{ic}\right)^2}} \tag{6a}$$

$$F_{r,x} = -\mu N \frac{\left(b + y_{ric}\right)}{\sqrt{\left(b + y_{ric}\right)^2 + \left(x_{ic}\right)^2}} \tag{6b}$$

$$F_y = -\mu N \left(\frac{x_{ic}}{\sqrt{\left(b - y_{lic}\right)^2 + \left(x_{ic}\right)^2}} + \frac{x_{ic}}{\sqrt{\left(b + y_{ric}\right)^2 + \left(x_{ic}\right)^2}} \right) \tag{6c}$$

where N_l, N_r are the normal forces between the track and climbing surface for the left and right tracks and typical values of x_{ic}, y_{lic}, y_{ric} are shown to be on the range of (0.15, 1.25, 1.25)*b, respectively (O'Toole and Canfield, 2010; Mandow et al., 2007). The track torque required to overcome this friction is,

$$\tau_l = rF_{l,x} \tag{7a}$$

$$\tau_r = rF_{r,x} \tag{7b}$$

Additional slipping results from travel on non-planar surfaces (Sreenivasan and Nanua, 1996) and is shown in Figure 6. Here, lateral slip is shown since the centre distance between the robot tracks is constant but the distance between the track paths shown in Figure 6 when measured along the y_{ro}-axis is variable. The amount of slip can be illustrated by calculating the distance between the track paths in the y_{ro} direction as follows. The slope at any point along the curve is $du_i(x)/dx$ and the curve tangent is $\tan^{-1}\left(du_i(x)/dx\right)$. The lateral distance, d_x, relative to a maximum distance, d, is given as follows:

$$\mathrm{d_x} = \mathrm{d}^{*}\cos\left(\tan^{-1}\left(du_i(x)/dx\right)\right). \tag{8}$$

This changing distance will contribute to increased slipping representing in the track instant centre parameters, x_{ic}, y_{lic}, y_{ric} and will impact track torques as shown in Eqs. (6) and (7). The size of torque for a representative prototype system with magnetic tracks producing 200 N attraction force and 10 cm radius drive sprockets was observed to range between + and −15 Nm of track torque. It is noted that this value is consistent with torque measurements taken from the experimental prototype presented in Section 3.

2.1.1 Kinematic control

In order to follow the paths defined in Section 2 and shown in Figure 4 (or Figure 6 for the unwrapped cylinder), a control strategy is suggested based on incremental basis along a reference trajectory following the method shown in Siegwart and Nourbakhsh (2004). The reference trajectory for the robot chassis is shown in Figure 4 and the goal is to define the inputs needed to trace the path given by an idealised, virtual robot that tracks the reference path given by coordinates $\left[\mathrm{x}_{ref} \quad y_{ref} \quad \theta_{ref}\right]$ in the unwrapped plane (Figure 6) with $y_{ref} = u$ and $\theta_{ref} = \tan^{-1}\left(du_i\left(x\right)/dx\right)$. The current error in position in the unwrapped plane is first determined as follows:

$$\Delta x = x_{\text{ref}} - x_{\text{current}} \tag{9a}$$

$$\Delta y = y_{\text{ref}} - y_{\text{current}} \tag{9b}$$

and then cast into a coordinate frame that defines the error in terms of distance (ρ), direction to reference position (α) and direction to reference orientation (β).

$$\rho = \sqrt{\Delta x^2 + \Delta y^2} \tag{10a}$$

$$\alpha = atan2\left(\Delta y, \Delta x\right) \tag{10b}$$

$$\beta = \theta_{ref} - \alpha \tag{10c}$$

A linear control scheme is now defined in the robot local frame as,

$$v_x = K_p * \rho \tag{11a}$$

$$\omega_z = K_\alpha * \alpha + K_\beta * \beta \tag{11b}$$

which form the two velocity inputs (linear and angular velocity) for the tracked vehicle. Siegwart and Nourbakhsh (2004) show that stability of a linearised control system of this type exists when $K_p > 0$, $K_\beta > 0$, and $K_\alpha - K_p > 0$.

2.2 Expanded robot model

An expanded model of a tracked SSMR travelling along the defined path is now proposed. This model will develop a kinematic estimation of the pose (position and orientation) of the left and right track modules based on a defined position of the chassis centre. To do this, the pose is determined according to a state of ‘Geometric stability’. Here, geometric stability is defined as a condition in which opposing, symmetric components of the robot are geometrically even in their positioning relative to the base

surface. This is achieved by placing the robot on the base surface in a manner such that keypoints are equally displaced from the surface (based on minimum distance). The pose of each track is defined by two keypoints (the exterior contact points of each track) and the surface. A vector along the line between these two points defines the *x*-axis of the track, while the surface normal is used to define the *z*-axis. The track frame origin is placed at a key point that defines the centre of the track in contact with the climbing surface. The keypoints are shown in Figures 2 and 3 and are found according to the process described here. The method is described for one of the track modules, but will be applied to each track in turn, where subscript $i = l$ for the left track, $i = r$ for the right track, MP_i denotes midpoints of the track frames, and EP_i denotes the end points of the track frames. This paper treats the kinematics in an instantaneous sense in that the defined state of geometric stability is only instantaneously representative of the vehicle.

The process of finding the track frames starts with keypoints $\mathbf{MP1}_i$, located at $\mathbf{MP1}_i = \mathbf{C} + \text{sign}(i)\frac{\text{b}}{2}\boldsymbol{y}_{ro}$, $\text{sign}(i) = 1,\ i = left,\ -1,\ i = right$. The keypoints $\mathbf{MP2}_i$ are found at the intersection of a line passing through $\mathbf{MP1}_i$ in the direction of $\mathbf{z}_\text{m}$ and the surface as

$$\mathbf{MP}2_i = \mathbf{MP}1_i - \text{u}_\text{M}\mathbf{z}_M \tag{12}$$

with

$$\text{u}_\text{M} = \frac{-\left((\boldsymbol{z}_M \cdot \mathbf{MP}1_i) - \text{z}_{M,3}MP1_{i,3}\right) \pm \sqrt{\left((\boldsymbol{z}_M \cdot \mathbf{MP}1_i) - \text{z}_{M,3}MP1_{i,3}\right)^2 - \left(1 - \text{z}_{M3}{}^2\right)\left(MP1_{i,1}^2 + MP1_{i,2}^2 - R^2\right)}}{1 - \text{z}_{M,3}{}^2} \tag{13}$$

$$\mathbf{MP}1_i = \begin{bmatrix} MP1_{i,1} & MP1_{i,2} & MP1_{i,3} \end{bmatrix}^T, \tag{14}$$

and $\mathbf{z}_M = \begin{bmatrix} z_{M,1} & z_{M,2} & z_{M,3} \end{bmatrix}^T$ a vector perpendicular to the line segment $\mathbf{MP1_1}$-$\mathbf{MP1_2}$ lying in the y_{ro}-z_{ro} plane.

The line segment $\mathbf{MP1_1}$-$\mathbf{MP1_2}$ is rotated about the x_{ro}-axis until the triangles $\mathbf{C}$-$\mathbf{MP1_1}$-$\mathbf{MP2_1}$ and $\mathbf{C}$-$\mathbf{MP1_2}$-$\mathbf{MP2_2}$ become mirrored, equal images (Figure 8a). This achieves geometric stability for track width about the robot roll axis. At point $\mathbf{MP2}_i$, an intermediate track frame ITF_i is defined as $[x_{ro},\ y_{ITFi},\ z_{ITFi}]^\text{T}$ where z_{ITFi} is the surface normal at $\mathbf{MP2}_i$ and y_{ITFi} completes the frame. The keypoints $\mathbf{EP1}_{\mathbf{frnt},i}$, $\mathbf{EP1}_{\mathbf{rear},i}$ are located at $\{\text{l}/2,0,0\}^\text{T}$ and $\{-\text{l}/2,0,0\}^\text{T}$, respectively, in the intermediate track frame ITF_i. The keypoints $\mathbf{EP2}_{\mathbf{frnt},i}$ $\mathbf{EP2}_{\mathbf{rear},i}$ are found at the intersection of a line passing through $\mathbf{EP1}_{\mathbf{frnt},i}$,$\mathbf{EP1}_{\mathbf{rear},i}$ in the direction of $\mathbf{z}_\text{E}$ and the surface as

$$\mathbf{EP}2_{frnt,i} = \mathbf{EP}1_{frnt,i} - \text{u}_E\mathbf{z}_E \tag{15}$$

$$\text{u}_E = \frac{-\left((\mathbf{z}_E \cdot \mathbf{EP}_{1,i}) - z_{E,3}\text{EP1}_{frnt,i,3}\right) \pm \sqrt{\left((\mathbf{z}_E \cdot \mathbf{EP}_{1,\text{i}}) - z_{E,3}\text{EP1}_{frnt,i,3}\right)^2 - \left(1 - z_{E,3}^2\right)\left(\text{EP1}_{\text{frnt},i,1}^2 + \text{EP1}_{\text{frnt},i,2}^2 - R^2\right)}}{1 - z_{E,3}^2} \tag{16}$$

$$\mathbf{EP}1_{frnt,i} = \begin{bmatrix} EP1_{frnt,i,1} & EP1_{frnt,i,2} & EP1_{frnt,i,3} \end{bmatrix}^T \tag{17}$$

Figure 8 (a) Rotation about x_{ro} and (b) rotation about y_{ITFi}

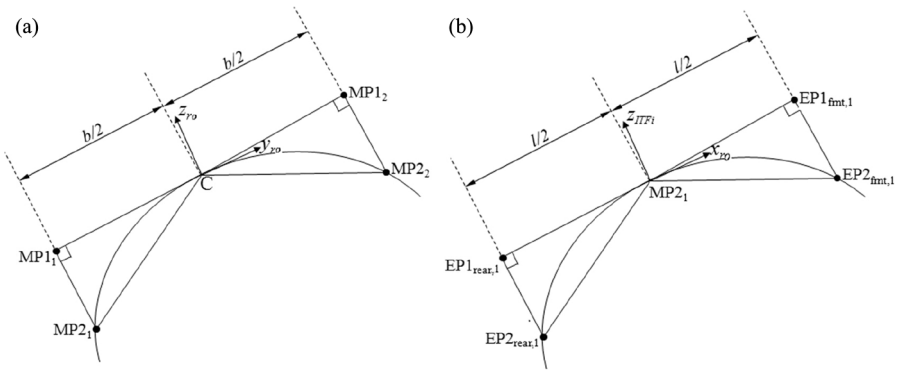

and $\mathbf{z}_E = \begin{bmatrix} z_{E,1} & z_{E,2} & z_{E,3} \end{bmatrix}^T$ a vector perpendicular to the line segment $\mathbf{EP1_{rear,}}_i$-$\mathbf{EP1_{frnt,}}_i$ lying in the y_{ITFi}-z_{ITFi} plane.

The line segment $\mathbf{EP1_{rear,1}}$-$\mathbf{EP1_{frnt,1}}$ is rotated about the y_{ITFi}-axis until the triangles $\mathbf{MP2_1}$-$\mathbf{EP1_{frnt,1}}$-$\mathbf{EP2_{frnt,1}}$ and $\mathbf{MP2_1}$-$\mathbf{EP1_{rear,1}}$-$\mathbf{EP2_{rear,1}}$ become mirrored, equal images (Figure 8b). Where $\mathbf{MP2_i}$ is the midpoint of the track frame and as seen in Figure 8b is located in the centre of the track frame end points **EP1** and **EP2**. This achieves geometric stability for track length about the pitch axis.

The track frame is defined as $[x_i, y_i, z_i]^T$ where x_i is the unit vector along the line segment $\mathbf{EP2_{rear,1}}$-$\mathbf{EP2_{frnt,1}}$ directed towards $\mathbf{EP2_{frnt,1}}$, $y_i = y_{ITFi}$ and z_i completes the frame. The origin of the track frame is located at $\mathbf{MP2}_i$. Note that the line connecting the track frame origins, $\mathbf{MP2_l}$–$\mathbf{MP2_r}$ is not parallel to $\mathbf{MP1_l}$–$\mathbf{MP1_r}$ as shown in Figure 9. This will imply lateral slip will occur between the left and right tracks for any case in which $\omega_l \neq \omega_r$ where ω_l, ω_r are the left and right track angular velocities as demonstrated in Sreenivasan and Nanua (1996), Chakraborty and Ghosal (2004).

Figure 9 Contact line ($MP2_l$-$MP2_r$) and axle line ($MP1_l$-$MP1_r$)

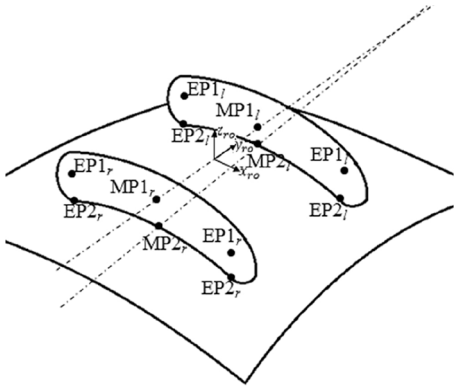

With the left and right track frames evaluated, the relative rotation between them is described with an SO(3) rotation operator **R**, defined in terms of the *z*-*y*-*x*, ϕ–θ–ψ, angles about moving axes yielding

$$\theta = \sin^{-1}\left(-R_{1,3}\right) \tag{18}$$

$$\psi = \text{atan2}\left(\frac{R_{1,2}}{\cos(\theta)}, \frac{R_{1,1}}{\cos(\theta)}\right) \tag{19}$$

$$\phi = \text{atan2}\left(\frac{R_{2,3}}{\cos(\theta)}, \frac{R_{3,3}}{\cos(\theta)}\right) \tag{20}$$

where R_{ij} is the row i, column j component of the rotation operator **R** and atan2 is the quadrant sensitive inverse tangent function.

3 Results and evaluation

This section now compares the proposed model with experimentally derived data to evaluate its validity. The model will then be considered over a large range of operating conditions to consider limiting behaviours of the system. To perform these tests, an experimental mobile robot climbing system is constructed for operating on non-planar surfaces. The experimental system is based on a simplified test platform of the track-based skid-steer mobile welding robot presented in (O'Toole and Canfield, 2010) and is shown in Figure 1. A prototype of this system was developed to fully encode and measure chassis suspension parameters on a system while being operated on curved surfaces of various scales. The prototype test robot is shown in Figure 10 and has kinematic parameters (as defined in Figure 2): b = 0.2032 m, l = 0.2286 m and is operating on a cylindrical tank with radius R = 2.0 m.

Figure 10 Prototype non-planar robot traversing cylindrical tank (see online version for colours)

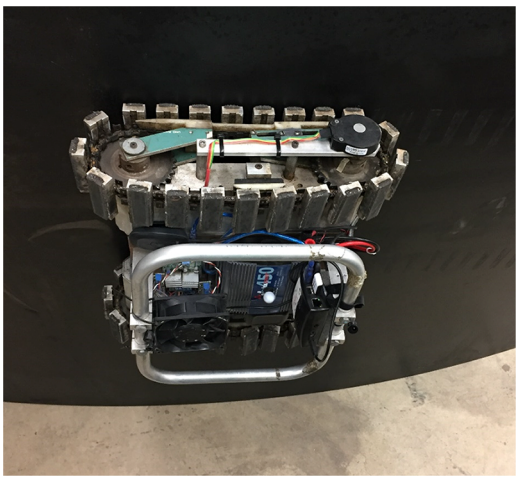

3.1 Model validation

The chassis provides relative roll and pitch mobility between the track units, where roll allows rotation about a longitudinal axis (parallel to the tracks) and pitch allows rotation about a transverse axis (orthogonal to the tracks). The roll and pitch degrees of freedom are encoded with 2500 count encoders and recorded through a Measurement Computing 8-Channel Quadrature Encoder using Matlab software. The data are recorded as the robot traverses candidate paths around a cylindrical steel tank constructed of a smooth, painted surface. The candidate paths are described as the intersection of a plane with the cylindrical surface and are created by projecting a laser plane onto the surface at prescribed angles to describe the path. A combination of rotary encoders and camera system is used to encode the location of the robot along the path. Figure 10 shows the test system in progress. This system provides a means to evaluate two expected motions (pitch and roll) required for traversing non-planar surfaces; however, the third expected motion (yaw or transverse slipping) is not evaluated.

The pitch, yaw and roll angles between the left and right track frames are evaluated from the expanded model (Section 2.2), while a separate set of collected data is replicated from empirical testing. The evaluated pitch and yaw angles from the expanded model are then compared to the collected data from experimental testing on a cylindrical tank. These tests are performed for three representative paths as shown in Figure 11a-c for $l' = 0.11$, $b' = 0.1$ and $\beta = 30°$, 60° and 80°, respectively. Where $l' = l/R$ is the non-dimensionalised length and $b' = b/R$ the non-dimensionalised width.

Figure 11 (a) Plot of pitch, yaw and roll over the path $\beta = 30°$. (b) Plot of pitch, yaw and roll over the path $\beta = 60°$. (c) Plot of pitch, yaw and roll over the path $\beta = 80°$

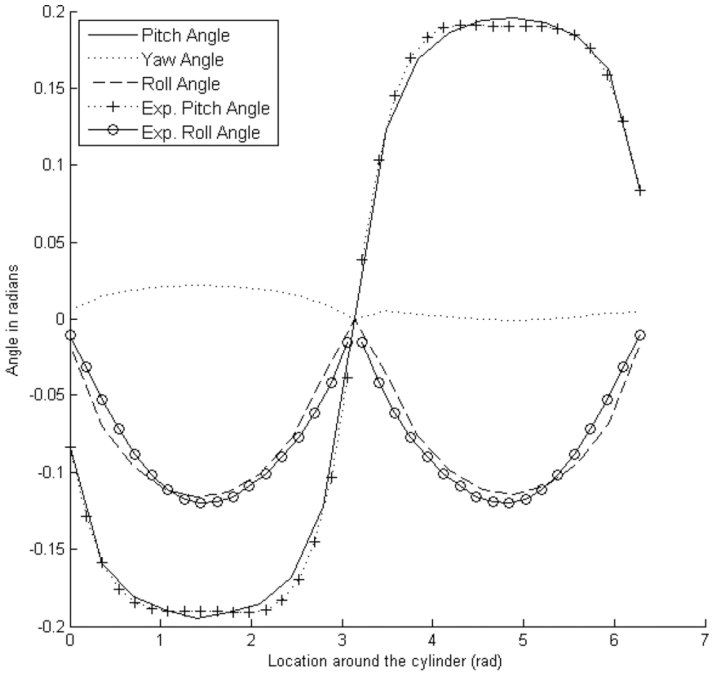

(a)

Figure 11 (a) Plot of pitch, yaw and roll over the path $\beta = 30°$. (b) Plot of pitch, yaw and roll over the path $\beta = 60°$. (c) Plot of pitch, yaw and roll over the path $\beta = 80°$ (continued)

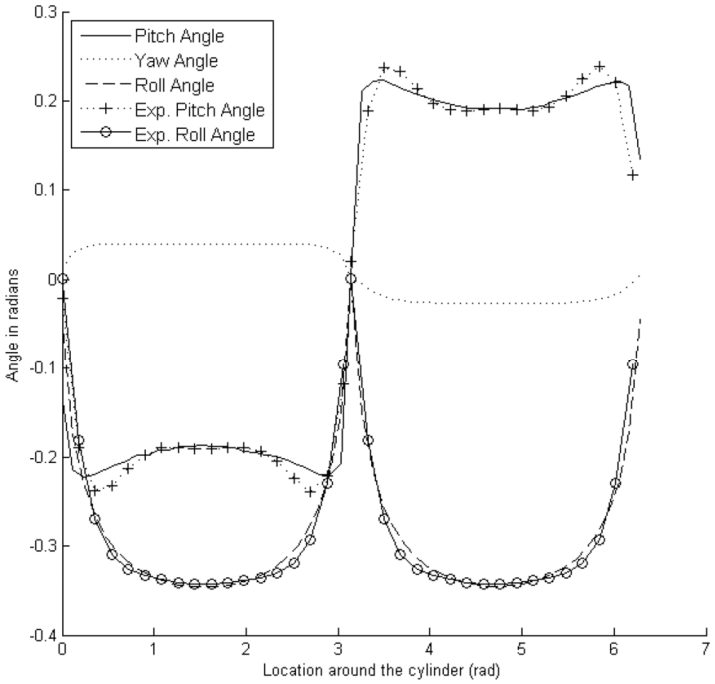

(b)

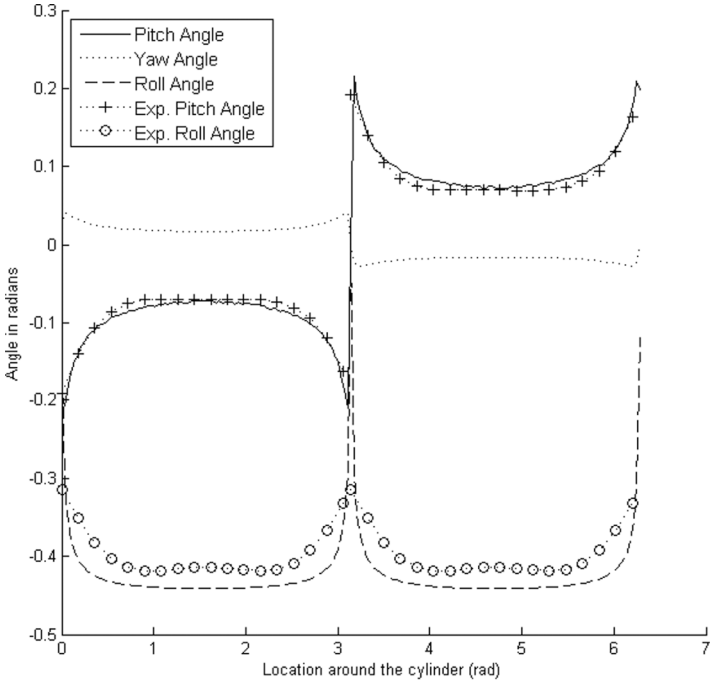

(c)

These data above show the positive correlation between the model-predicted pitch, roll and the experimentally collected pitch and roll data for all three cases. The average error is determined for each path in which the average error is presented as the sum of square error taken over the path and divided by the length of the path with results shown in Table 1. The overall error results show that the model prediction provides good correspondence for the pitch and roll. While it is most accurate for paths with lower inclinations the error increases slightly as the inclination increases, with the largest inclination evaluated as $\beta = 80°$.

Table 1 Pitch and roll candidate path error

Candidate path	*Pitch (% error)*	*Roll (% error)*
30	1.7	0.9
60	2.2	1.8
80	6.4	7.1

3.2 Parametric analysis

Finally, the expanded model is applied to the tracked SSMR over a range of sizes of the robot length, width and radius of the base surface to numerically evaluate its behaviour and search for any limiting conditions. The following cases describe a range of possible results for the pitch, roll and yaw as the robot-to-tank ratio goes from very small (relative to tank) to large. The maximum values of pitch, yaw and roll resulting between the left and right tracks are recorded for each path, and are plotted for a range of paths as, β is evaluated over a range from 0 to 90°. These results are all based on the expanded model (Section 2.2) which has been shown in Section 3.1 to be reasonably well validated. The results are provided in the following figures for $l' = 1 - 0.1$, $b' = 1.5$. Observations on this data are provided in Section 4.

4 Discussion

Two models were presented to consider the track-based SSMR operating on non-planar surfaces. The idealised model, based on the assumption that the SSMR is small relative to the curvature of the surface, shows a constant orientation between the tracks for any path consistent with the locally planar surface and exhibits no lateral slipping. The expanded model shows the robot to be in a constant state of turning for the majority of paths, with a purely sinusoidal path demonstrated when following the intersection of the projective path plane with the cylindrical base surface. The SSMR following the path defined by the expanded model further exhibits relative lateral slip between the left and right track surfaces.

The expanded model shows that the track modules of the SMR undergo a combination of pitch, yaw and roll motion when travelling along any of the defined paths, except for the extreme cases in which the projective path plane is orthogonal or parallel to the vertical axis of the base surface. As the robot dimensions are reduced relative to the

base surface dimension, such as a small robot operating on a very large diameter surface, the expanded model results approach those of the idealised model as shown in Figure 12a-c. As the robot dimensions become larger relative to the base surface, for example, a robot operating on a small diameter tank or pole, the relative rotations between the tracks become significant. The expanded model further shows that the track units undergo relative lateral slip and that the slip is greater than that for the small robot assumption. This is consistent with the results presented for WMR on uneven terrain (Davis et al., 1997; Sreenivasan and Nanua, 1996). It has been shown that turning of SSMRs requires large torque inputs for any rate of turn (Mandow et al., 2007). This implies that any defined path on a non-planar surface (except for special cases, such as β orthogonal or parallel to vertical axis in this model) will require large torque inputs over the entire path. Conversely, the paths that would result in low torques would be of a helix shape for the cylindrical base surface considered in this paper.

Figure 12 (a) Plot of pitch over a range of paths. (b) Plot of yaw over a range of paths. (c) Plot of roll over a range of paths

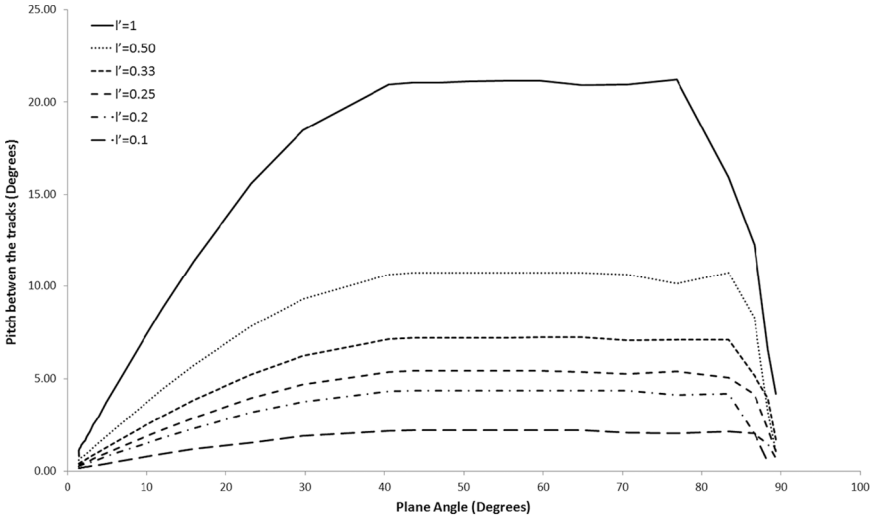

(a)

Figure 12 (a) Plot of pitch over a range of paths. (b) Plot of yaw over a range of paths. (c) Plot of roll over a range of paths (continued)

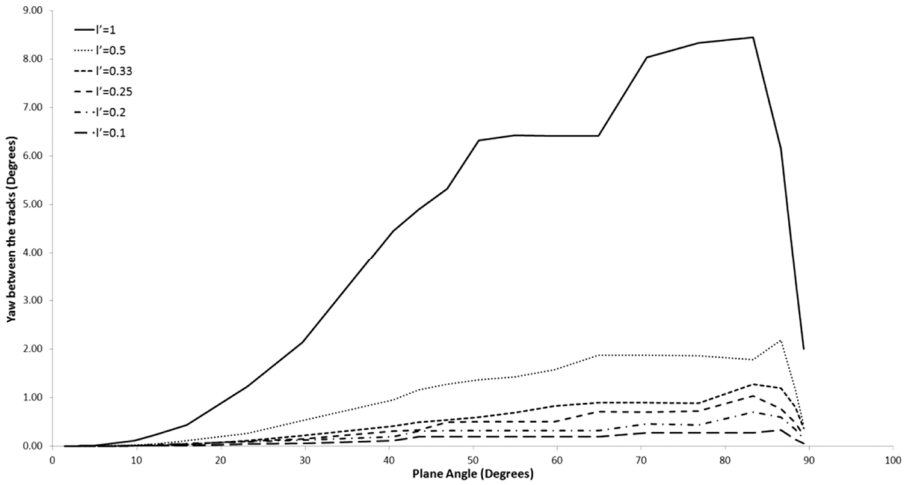

(b)

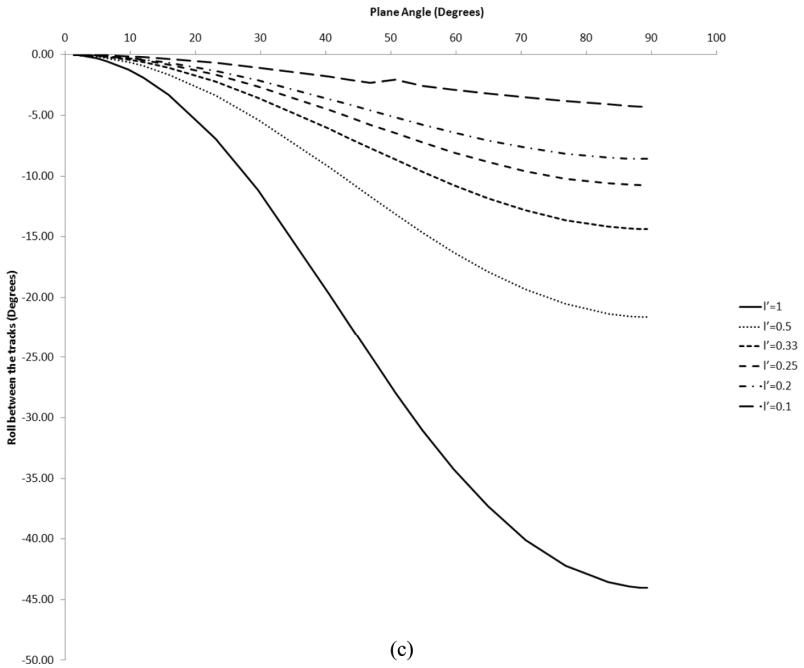

(c)

The plots given in Figure 11 a-c describe the behaviour of the pitch, yaw and roll rotations between the left and right axes for three candidate paths, β = 30°, 60°, 80°. Figure 11a-c was then overlaid with experimentally collected pitch and roll data for comparison between the empirical and experimentally collected roll and pitch data. It can be seen from these Figures that the expanded model provides good measure of the pitch and roll evaluation and the experimentally collected data. There are, however, slight deviations in the data collected and the model prediction such as the collected pitch and

roll exhibiting slightly larger or smaller measurements. The deviations in the pitch and roll indicate that there were relatively greater and smaller pitch and roll motion experienced at certain locations by the rotary encoders than was initially predicted by the expanded model. It is possible that these deviations are accurate measures of the behaviour of the pitch and roll at those locations on the tank. However, it may also be attributed to the experimental test environment conditions, encoder accuracy, or possibly the surface conditions of the tank. The error results, including the slight deviations, do however show that the expanded model prediction provides good correlation for the pitch and roll and is most accurate for paths with lower inclinations and increases slightly as the inclination increases. These plots indicate that the through using the expanded model a relatively accurate estimation of the roll and pitch of the system can be achieved and used in kinematic design of mobile robotic platforms on non-planar surfaces.

The plots in Figure 12a-c evaluate a range of the maximum pitch yaw and roll rotations between the left and right tracks as the size of the robot parameters, length, width and radius of the base surface are altered. These plots provide information that can be used to provide design limitations of a track-based SSMR robot system for operation on non-planar surfaces with different design parameters. For example, when given information on the curvature of the climbing surface, the amount of relative rotation required between the left and right tracks is defined over a range of robot platform sizes in Figure 12. In a similar manner, when a given robot is expected to operate over a range of climbing surfaces of different size, Figure 12 defines the range of relative motion required between the left and right tracks. This rotation is required to achieve full contact of the track with the surface as it traverses the surface.

5 Conclusion

This paper has examined the motion of tracked-based SSMRs following a path on a class of non-planar surfaces. The path was defined as the intersection of a plane, called the projective path plane with the base surface. The paper examined both a simplistic or idealised, small robot assumption and an expanded model that defines the robot pose according to uniform distribution of suspension displacements of the robot. The model is evaluated over a range of sizes of base surfaces and a range of robot dimensions. It is shown that for both models, relative lateral slipping between the left and right tracks occurs along the paths. Furthermore, it is shown from the expanded model that three rotational degrees of freedom between the left and right tracks are required to maintain a uniform distribution of suspension displacements along the path. These results are intuitive and expected for relative pitch and roll motions (rotations about the robot longitudinal and lateral directions). The results also show relative yaw motions between the tracks, which contributes to relative lateral slipping as the robot operates along a prescribed path on non-planar surfaces. The resulting model can be used in the kinematic design of tracked-based SSMRs for operation on non-planar surfaces. It can also be used to help predict the operational torques required for the combination of lateral slipping and turning defined over the moving path. This model presents a step forward in developing improved robots for performing manufacturing tasks in unstructured environments.

References

Apostol, T.M. and Mnatsakanian, M.A. (2007) 'Unwrapping curves from cylinders and cones', *The Mathematical Association of America*, Monthly 114, May.

Chakraborty, N. and Ghosal, A. (2004) 'Kinematics of wheeled mobile robots on uneven terrain', *Mechanism and Machine Theory*, Vol. 39, pp.1273–1287.

Davis, P.W., Sreenivasan, S.V. and Choi, B.J. (1997) 'Kinematics of two wheels joined by a variable length axle on Uneven Terrain', *ASME 1997 International Design Engineering Technical Conferences*, DETC97/DAC-3857, Sacramento, September 14–16.

Fischer, W., Tache, F. and Siegwart, R. (2008) 'Magnetic wall climbing robot for thin surfaces with specific obstacles', *Field and Service Robotics*, Vol. 42, pp.551–561.

Hoggins, J. (1988) 'Legged robots on rough terrain: experiments in adjusting step length', *Proc. 1988 IEEE International Conference on Robotics and Automation*, New York, NY, pp.824–826.

Kim, H., Kim, D. and Yang, H. (2008) 'Development of a wall-climbing robot using a tracked wheel mechanism', *Journal of Mechanical Science and Technology*, Vol. 22, pp.1490–1498.

Kumar, P., Hill, T., Bryant, D.A. and Canfield, S.L. (2011) 'Modeling and design of a linkage-based suspension for tracked-type climbing mobile robotic systems', *Proc. ASME 2011 International Design Engineering Technical Conferences*, DETC2011-48555, pp.827–834.

Letourneau, D. and Arsenault, M. (2003) 'AZIMUT, a leg-track-wheel robot', *Proc. 2003 IEEE/RSJ International Conference on Intelligent Robots and Systems.*

Mandow, A., Martinez, J.L., Morales, J., Pedraza, S. and García-Cerezo, A. (2005) 'Approximating kinematics for tracked mobile robots', *International Journal of Robotics Research*, Vol. 24, No. 10, pp.867–878.

Mandow, A., Martinez, J.L., Morales, J., Blanco, J., Garcła-Cerezo, A.J. and Gonzalez, J. (2007) 'Experimental kinematics for wheeled skid steer mobile robots', *Proc. IEEE/RSJ Int. Conf. Intelligent Robots Syst*ems, San Diego, CA, pp.1222–1227.

O'Toole, A.T. and Canfield, S.L. (2010) 'Developing a kinematic estimation model for a climbing mobile robotic welding system', *ASME 2010 International Design Engineering Technical Conferences*, DETC2010-28878, pp.1187–1194.

Raibert, M. and Blankespoor, K. (2008) 'BigDog, the rough-terrain quadruped robot', *Proc. 17th World Congress; The International Federation of Automatic Control*, Seoul, Korea, July 6-11.

Shen, W., Gu, J. and Shen, Y. (2005) 'Proposed wall climbing robot with permanent magnetic tracks for inspecting oil tanks', *2005 IEEE International Conference on Mechatronics and Automation*, Vol. 4, pp.2072–2077.

Sreenivasan, S.V. and Nanua, P. (1996) 'Kinematic geometry of wheeled vehicle systems', *ASME 1996 Design Engineering Technical Conferences*, 96-DETC-MECH-1137, Irvine, CA.

Siegwart, R. and Nourbakhsh, I.R. (2004) *Introduction to Autonomous Mobile Robots*, MIT Press.

Xu, Z. and Ma, P. (2002) 'A wall-climbing robot for labelling scale of oil tank's volume', *Robotica*, Vol. 20, pp.209–212.

Yan, W., Shuliang, L., Dianguo, X., Yanzheng, Z., Hao, S. and Xueshan, G. (1999) 'Development & application of wall-climbing robots', *Proceedings of the IEEE International Conference on Robotics and Automation* (ICRA'99), Detroit, MI, USA, pp.1207–1212.